



This is the accepted manuscript made available via CHORUS. The article has been published as:

## Reduced mixing in inertial confinement fusion with early-time interface acceleration

C. R. Weber, D. S. Clark, D. T. Casey, G. N. Hall, O. Jones, O. Landen, A. Pak, and V. A. Smalyuk

Phys. Rev. E **108**, L023202 — Published 16 August 2023

DOI: [10.1103/PhysRevE.108.L023202](https://doi.org/10.1103/PhysRevE.108.L023202)

# Reduced Mixing in Inertial Confinement Fusion with Early-time Interface Acceleration

C. R. Weber,<sup>1</sup> D.S. Clark<sup>1</sup>, D.T. Casey<sup>1</sup>, G.N. Hall<sup>1</sup>, O. Jones<sup>1</sup>, O. Landen<sup>1</sup>, A. Pak<sup>1</sup>, V.A. Smalyuk<sup>1</sup>

<sup>1</sup>Lawrence Livermore National Laboratory, P.O. Box 808, Livermore, California 94551-0808, USA

(Received ; published )

In inertial confinement fusion (ICF) implosions, the interface between the cryogenic DT fuel and the ablator is unstable to shock acceleration (the Richtmyer-Meshkov instability, RM) and constant acceleration (Rayleigh-Taylor instability, RT). Instability growth at this interface can reduce the final compression, limiting fusion burn-up. If the constant acceleration is in the direction of the lighter material (negative Atwood number), the RT instability produces oscillatory motion that can stabilize against RM growth. Theory and simulations suggest this scenario occurred at early times in some ICF experiments on the National Ignition Facility, possibly explaining their favorable performance compared to 1D simulations. This characteristic is being included in newer, lower adiabat designs, seeking to improve compression while minimizing ablator mixing into the fuel.

DOI:

To ignite and burn an inertial confinement fusion (ICF)[1], [2] target, the deuterium-tritium (DT) fuel must be compressed to high areal densities to confine the hot-spot and give time for fusion alpha-particles to heat and boot-strap the ignition process. Experience with ICF designs on the National Ignition Facility (NIF)[3]–[5] that use high-density carbon (HDC)[6], [7] (diamond) ablators has, however, not shown the expected compression increase between designs that seek to lower the entropy of the fuel[8]. A possible reason is due to mixing at the fuel-ablator interface[9]–[11], which can heat the fuel, increase its entropy, limit the final compression, and ultimately reduce the fuel burn-up. In this work we show a new stabilizing mechanism that may have aided the compression of some ICF designs: an interface experiencing constant acceleration following the shock-breakout can have significantly less perturbation growth than without this acceleration. Designs that incorporate this technique can potentially improve compression while minimizing ablator mixing into the DT fuel, allowing for higher target gains to be achieved.

In ICF, the laser pulse is tailored to send a series of shock waves to compress the cryogenic deuterium-tritium (DT) fuel. Since an individual shock wave can only compress the fuel by up to 4x from its initial 0.25 g/cm<sup>3</sup>, separating the shocks into 2-4 carefully timed shocks can combine for a larger compression[12]. Unexpectedly, however, two designs frequently used on NIF that have 2 or 3 shocks crossing through the ice exhibit very similar levels of compression[8]. These designs are shown in Figure 1. Both designs use an HDC ablator and have 3 steps in the laser pulse, sending 3 shock waves. Typical shock timing is used in the “HDC” design with the 3 shocks timed to traverse the cryogenic DT ice separately before merging near the ice-gas interface[11], [13]. This shock-timing strategy is the same as used in the larger-scale “Hybrid-E” design that achieved a burning and igniting plasma[14]–[18]. The “Big-foot” design[19]–[21] deliberately merges the first two shocks prior to their reaching the ice, so the ice only senses two shocks, the first one very strong, and is therefore on a higher adiabat (where adiabat is the ratio of the pressure to the Fermi degenerate pressure[22] and is a measure of the fuel’s entropy).

Implosions with a lower adiabat (entropy) following the shock traversals can compress greater during the final stagnation phase. Simulations expect the HDC design to have an adiabat of 3 at the time of peak implosion velocity, while the Big-foot design’s adiabat is 4.2. In experiments, the compression of the fuel is measured by the down-scattered ratio (DSR) of scattered-to-primary DT fusion neutrons and approximately related to the fuel areal density by  $\rho R_{fuel} \approx 19DSR$ . This DSR was simulated to be 3.9% for HDC and 3.2% for Big-foot, but both experiments recorded  $3.1 \pm 0.2\%$  (NIF experiments N170827 and N180128).

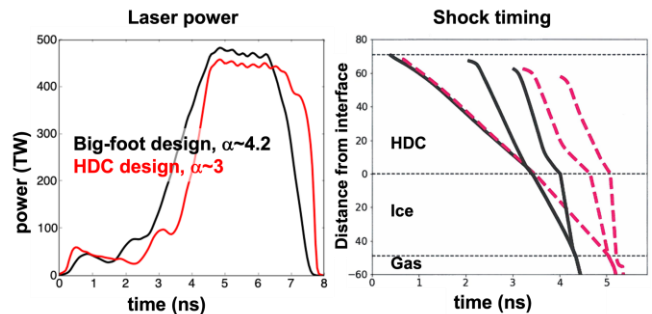


FIG 1 (a) Laser pulse history and (b) shock wave trajectory in Lagrangian coordinates for the Big-foot and HDC designs. Both designs have 3 shocks but in the Big-foot design the first two shocks are timed to merge prior to entering the ice, increasing the entropy of the fuel. The final shock is designed to merge near the ice-gas interface

A possible reason for the reduced compression in the HDC design is material mixing at the fuel-ablator interface. Mixing of ablator material into the dense DT fuel will heat the fuel, increasing its entropy and reducing its final compression[9], [11], [23], [24]. This picture is supported by high-resolution 2D simulations. Figure 2 shows simulations using Hydra[25] to model a 8 degree wedge at the equator with 0.004 degree/zone resolution and includes surface roughness and a model of HDC’s microstructure[26], [27]. This simulation assumed an HDC grain size of 2 micron and de-resolved the 4 nm interstitials to 200 nm, conserving mass,

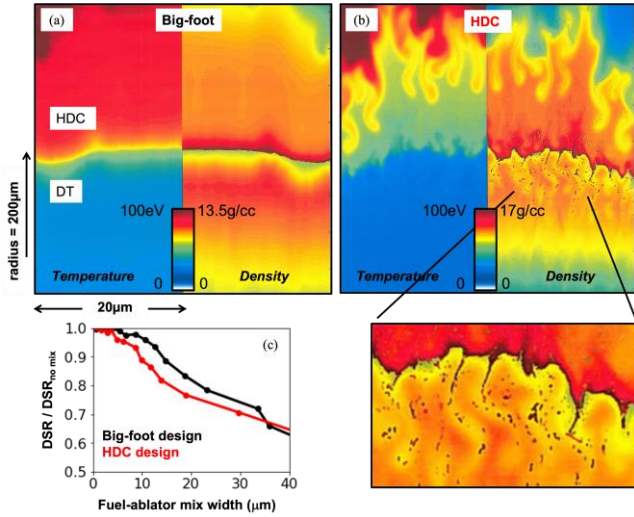


FIG 2 Density and temperature at the fuel-ablator interface in high-resolution 2D simulations at radius 200 micron in the (a) Big-foot and (b) HDC designs. Times are 7.50 ns and 7.68 ns for (a) and (b). Big-foot appears very stable at this interface while with the HDC design there is ablator material mixing into the DT fuel. The impact of mix on DSR is shown in (c) from 1D simulations with an in-flight fall-line mix model turned on at various times.

but may under-predict the full extent of the mixing[28], [29]. These simulations are near the time of peak fuel velocity at radius 200 micron (convergence ratio  $\sim 4.5$ ), prior to the stagnation shock slowing down the shell. The HDC design experiences fine-scaled mixing of ablator material into the DT. As this hot carbon mix enters the ice, it locally heats the surrounding DT and lowers its density. In contrast, the Big-foot design has no fine-scale mixing occurring at this interface.

The impact of these levels of mixing on compression is estimated using 1D simulations with a “fall-line” mix model, which allows the mix level to be adjusted to account for higher amounts of mixing that may occur in experiments. This model does not produce a predictive level of mix, as the user needs to specify when mixing starts, and the simulation will then mix across the interface based on the distance it has accelerated beyond its free-fall location. In this configuration, we are mixing during the in-flight acceleration period, rather than the late-time deceleration period used by others[30]. This model, in its implementation in Hydra, runs in-line, mixing materials and updating the equation of state as the simulation evolves, but the mixing does not respond dynamically to these changes, as the mix-width is solely prescribed by the fall-line distance. Other models, like RANS-based models[31]–[33] or buoyancy-drag models[34]–[36], can dynamically respond based on local changes to the Atwood number or sound speed. Figure 2(c) shows simulations with mixing turned on at various times, finding compression dropping for both designs as the fuel-ablator mix width is increased. The mix-width in this figure is measured at the time of peak velocity, 7.80 ns for HDC and 7.60 ns for Big-foot. At  $\sim 20$  microns of mix-width (similar to that seen in Figure 2(b)), the DSR drops to 80% of its original value for both designs. Interestingly the HDC design is

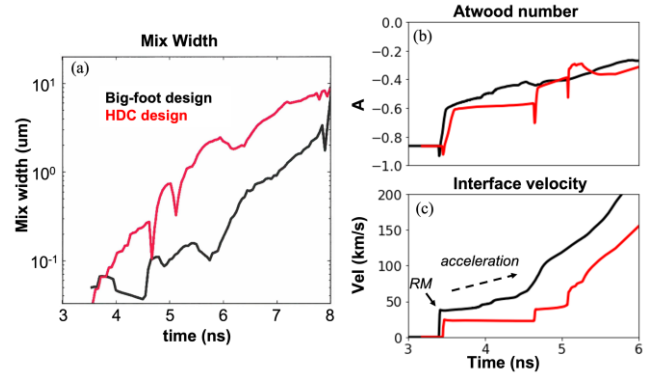


FIG 3 (a) Mix-width from the simulations in Figure 2. The mix-width is the extent that ablator material goes from 0.1% to 99.9% at the fuel-ablator interface. (b) Atwood number vs time and (c) Fuel-ablator interface velocity. The difference in mix-width is apparent immediately and appears to be due to the initial RM growth, as during this time the Atwood numbers are negative (stable) for both designs. The main difference is that there is a near constant acceleration in the Big-foot design following the initial shock breakout.

degraded more for a given level of mix because the lower adiabat results in a thinner fuel layer at peak velocity (25 microns vs 39 microns for Big-foot), thus more of the fuel is contaminated.

The traditional view of stability at this interface has been related to the classical Rayleigh-Taylor (RT) instability[37]–[40], where mixing would occur if the HDC ablator were lower density than the DT fuel in-flight, but these simulations suggest these densities are very similar and a different mechanism is responsible for the mixing dynamics.

To understand the cause of the mix-width difference between these two designs, we look at the time history of the mixing layer, shown in figure 3. The mix width of these two designs diverge immediately following shock breakout at 3.4 ns. At this early time, the interface is stable to Rayleigh-Taylor growth, as shown in Figure 3(b), due to its negative Atwood number ( $A = (\rho_{abl} - \rho_{DT}) / (\rho_{abl} + \rho_{DT})$ ), comparing the density between the ablator and DT). Both designs experience an impulsive acceleration which will lead to growth from the Richtmyer-Meshkov (RM) instability[41], [42], but we see in Fig. (3c) that the Big-foot design is further accelerating following the shock breakout whereas the HDC design has a constant velocity. This acceleration difference appears to be the cause of the mix-width divergence.

The impact of constant interface acceleration following the impulsive RM growth can be understood by considering the dispersion equation for an interface perturbation of height  $h$  and frequency  $\gamma^2 = Agk$ , where  $g$  is the acceleration and  $k$  is the wavenumber[43]:

$$\frac{\partial h^2}{\partial t^2} - \gamma^2 h = 0 \quad (1)$$

For a constant  $\gamma$  this has the solution

$$h(t) = h_0 \cosh(\gamma t) + \frac{\dot{h}_0}{\gamma} \sinh(\gamma t) \quad (2)$$

When  $Agk < 0$ , like the initial stage of these designs, where the abator is much denser than the DT fuel, this equation has oscillatory sine and cosine solutions,

$$h(t) = h_0 \cos(\gamma t) + \frac{\dot{h}_0}{\gamma} \sin(\gamma t) \quad (3)$$

The initial growth rate can be approximated by the impulsive RM formula  $\dot{h}_{0,RM} = \nabla V A k h_0$ , where  $\Delta V$  is the jump in interface velocity caused by the shock. Using the values similar to Figure 3,  $A = -0.5$ ,  $g = 20$  micron/ns<sup>2</sup>, and a 2 micron wavelength, Figure 4 shows the time history expected for a perturbation with and without a constant acceleration following the RM impulse of  $\dot{h}_0/h_0 = -63\text{ns}^{-1}$ . The oscillatory behavior of the constant acceleration limits the RM growth to a maximum amplitude of  $h_0\sqrt{1 + \Delta V^2 A k/g}$ . Figure 4(b) shows the growth factor ( $h/h_0$ ) after 1 ns following the initial shock acceleration for a range of mode numbers ( $k$ \*radius). This is approximately the time the second shock wave arrives, which will amplify any perturbations that grown during the first phase. The growth factor of low mode numbers is relatively unchanged, but by mode 200 the growth starts to reduce and inverts by mode 1000, with another inversion occurring at higher modes. This picture suggest that designs can aim to place the growth factor zero at the most dangerous mode, for example ablators like HDC and Be that have crystalline structure can time the growth-factor at the grain scale to be zero when the second shock arrives. The 2 micron grain scale used in the simulations of Figure 2 induce a mode  $\sim 3000$  perturbation, nearing one of the zeros in this growth-factor curve. The stabilizing effect RT can have on RM has been recognized elsewhere, particularly in experiments that are trying to achieve pure RM but must account for acceleration effects[44]–[48].

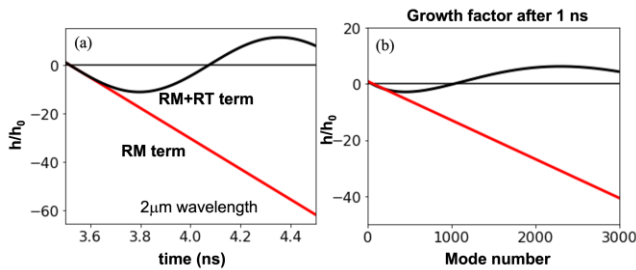


FIG 4 (a) Interface growth vs time following a Richtmyer-Meshkov (RM) interaction (red) or RM followed by Rayleigh-Taylor (RT) acceleration. The acceleration imparts an oscillation, limiting the unbounded RM growth. (b) Growth factor after 1 ns for a spectrum of mode numbers. Above mode 200 the growth factor is reduced with the acceleration term, with a zero near mode 1000.

We performed 2D ICF implosion simulations with single-mode perturbations to test this predicted oscillatory behavior in this more complicated scenario with time-varying

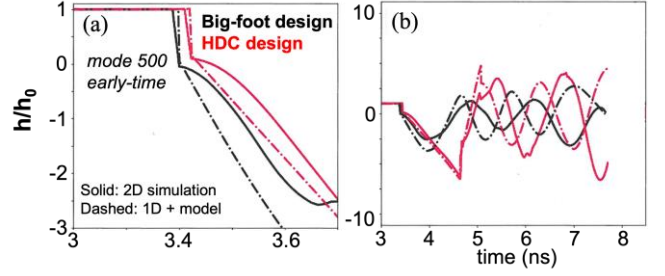


FIG 5: Growth factors from a mode 500 simulation (a) at early time and (b) up until peak velocity. At early time, the model accurately reproduces the compression and the growth rate, though sound-speed effects in the 2D simulation cause some delay that impacts the phase later in time. The model predicts a similar amplitude later in time, showing that mode 500 growth is minor at this interface.

accelerations and densities. These calculations impose a very small (0.01 nm) sine-wave perturbation at the fuel-ablator interface and track its amplitude growth through time. To analytically compute the RM growth rate, the impulsive growth-rate formula of Ref. [49] was used, which incorporates compressibility effects by averaging the post (+) and pre-shock (−)  $A$  and  $h$ ,

$$\frac{dh}{dt} = \frac{1}{2} k \Delta V (A^+ h_0^+ + A^- h_0^-)$$

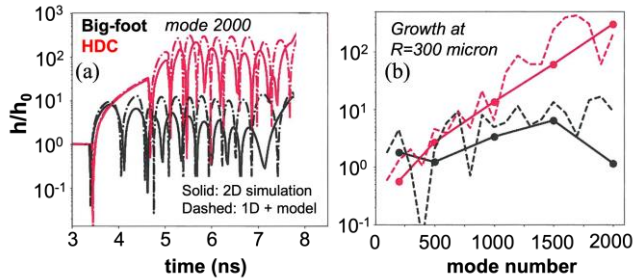
The post-shock amplitude is computed per Ref. [41], by noting that the shock of speed  $U_s$  will reach the peak of the perturbation first, accelerating it to a velocity of  $\Delta V$  over a time  $h_0/U_s$  before reaching the trough. Therefore, the amplitude will reduce to

$$h_0^+ = h_0^- \left(1 - \frac{\Delta V}{U_s}\right)$$

The pre and post-shock Atwood numbers are computed through 1D simulations like shown in Figure 3. To combine RM and RT effects in our analytical expression, equation 1 is augmented as

$$\frac{d^2 h}{dt^2} = \begin{cases} \frac{1}{2} k \Delta V (A^+ h_0^+ + A^- h_0^-) \delta(t) & \text{RM} \\ \gamma^2 h & \text{RT} \end{cases} \quad (4)$$

where the RM acceleration term is used if large interface accelerations are detected. For simplicity, this analysis omits Bell-Plessett[50], [51] effects, which can become important at late times. This equation is numerically integrated from the 1D simulations. Figure 5(a) shows this analytical model compared to the 2D perturbation simulation during the initial RM interaction. The interface amplitude compresses by  $\sim 10\times$  and then grows in the negative direction. This 1D model accurately reproduces the growth-rate, but the 2D simulations show a start-up delay before reaching their linear rate. This delay is due to the finite time (wavelength/sound-speed) required for the baroclinic vorticity to communicate with the peak and trough of the perturbation[52]. One could add this delay time to this model, but it adds more complexity and is not needed for higher modes. Figure 5(b) shows that later in



time, this simple model has approximately reproduced the amplitude and periodicity of this mode 500 perturbation, but

FIG 6 Growth factor ( $h/h_0$ ) (a) vs time at mode 2000 and (b) vs mode number. The model reproduces the observed behavior, where the HDC design (red) shows significantly more growth than Big-foot (black) at modes above 1000.

small differences have accumulated and the two curves are out-of-phase. At this mode number the two designs show a similar growth factor of 3-6x. This level of growth is minor given the sub-micron perturbations present on these capsules.

At high mode numbers, where the RM growth is larger but the oscillatory impact of the RT term can reduce the overall growth, these two designs have significantly different growth factors. Figure 6(a) shows a 2D simulation with a linear mode 2000 perturbation compared to this analytical model. The model again does a good job at matching the early-time growth, the periodicity, and the approximate magnitude, but some small differences again accumulate. At late times (7-8 ns), the growth factors of these two designs differ by  $\sim 20$ -50x. Despite the detailed differences between the model and the 2D simulation, it is clearly useful for differentiating designs that will incur high-mode growth from those that remain stable (Figure 5(d)). The compute cost of this model from a 1D simulation is  $\sim 10^5$ x less than the 2D simulation shown in figure 2, so there is clear value in using this when doing initial design scoping. The growth factor spectrum (Figure 6(b)) using this model compared to a set of 2D calculations both show a similar picture as our simple estimate from Figure 2, where the stabilization from RT keeps the Big-foot growth factors low.

To predict the mix-width, the growth-factor estimations from this model need to be combined with the seeds on the capsule. While the roughness of many ablators is small at the very-high wavenumbers that are considered here, internal or isolated defects can imprint perturbations on the interface at all mode numbers. The typical concern with isolated defects is that they can inject a jet into the hot-spot[53], [54], but if there are significant numbers of them, like with HDC's micro-structure, they can couple to high-modes and the mechanisms discussed here can contribute to fuel-ablator mixing. Once the growth becomes nonlinear ( $kh \sim 1$ ) mode-coupling, bubble-merger, and other mechanisms will come into play, changing the growth rate from these linear predictions[55]–[58].

The reason for the initial accelerating interface in the Big-foot pulse is explored in Figure 7, showing pressure profile as the shocks moves through the ablator at four times. In the first three times we see the first shock with a flat  $\sim 11$  Mbar

pressure profile behind it. Shock 2, however, is followed by a steep gradient in pressure. This is due to the radiation drive history: despite the near flat laser power in the second pulse (2-3 ns), the radiation temperature is increasing in time as the hohlraum albedo is increasing as energy is stored in walls. Since the ablation pressure scales as  $P_{abl} \propto T^{3.5}$ , the rising ablation pressure will lead to a pressure gradient between the shock and the ablation front and will ultimately cause the interface to accelerate when shock 2 overtakes shock 1 before breaks out into the DT ice.

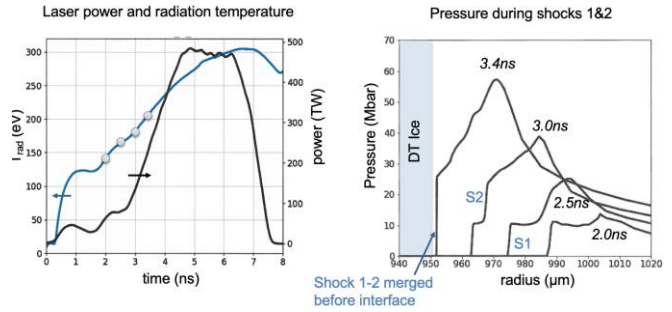


FIG 7 (a) Radiation temperature and laser power history for the Big-foot design. (b) Pressure profiles at for times prior to the shock reaching the DT ice, with times also marked in (a). The first pulse as a flat  $T_r$  history and the shock has flat trailing pressure profile, but the second shock has a ramped trailing pressure profile, owing to the increasing  $T_r$  history in the drive. This pressure gradient is what causes the interface acceleration when the merged first and second shocks merge and accelerate the interface.

The ramped pressure profile of Figure 7 gives guidance on how designs can seek a lower adiabat like HDC but retain the stabilizing characteristics of Big-foot. Two strategies are apparent: tailor the first shock so that it has an increasing pressure profile behind it to further accelerate the interface after breakout, or reduce the strength of the 2<sup>nd</sup> shock in Big-foot but keep its pressure gradient and shock 1-2 merge time. The first strategy has the greatest potential, as a single shock can be near the limit of HDC's melt pressure[59] and deposit less entropy than two shocks, but is likely more difficult to achieve, as a time dependent laser profile will need to be specified to accelerate the interface in the presence of EOS and hohlraum-dynamics uncertainties. The current "SQ-n" campaign on NIF is including this technique and others in a focused effort to increase compression in HDC implosions with minimal instability growth[60] and its interface acceleration history is being measured using a new refraction enhanced radiography technique[61]. Preliminary results of these experiments suggest that this strategy successfully improved the compression[62]. Figure 8 shows an example of the second strategy, where the drive flux in the second shock of Big-foot is reduced by 0.7x. The 3<sup>rd</sup> shock is also delayed to preserve the shock-timing strategy, with shocks 1 & 2 still merging in the ablator and the 3<sup>rd</sup> shock merging near the ice-gas interface. This weaker merged shock reduced the adiabat of Big-foot from 4.2 to 2.8, increasing its 1D yield by 5x. The 1D stability metric is shown in Figure 8(b), but to reduce the oscillations the growth-factors for modes 1500-2000 are averaged. This shows that this Big-foot design with

a lower second shock has better early time stability as the original Big-foot design. Later in time at 8 ns this new design experiences more growth due to a slightly unstable Atwood number (0.07 vs 0.0 for Big-foot). This design did not change the capsule properties, which could be further optimized by increasing the dopant to improve the Atwood number. A high-mode simulation of this design, shown in Figure 8(c) shows that the fuel-ablator mixing is similar to Big-foot and much less small-scale growth than in HDC.

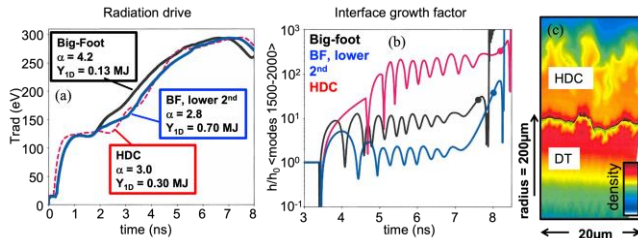


Figure 8 (a) Radiation drive history including an improved design (blue) that lowers the second shock pressure but preserves its stabilizing characteristics. (b) the growth factors, averaged over modes 1500-2000, show similar stability as Big-foot. (c) A high-resolution 2D simulation shows that the interface is more stable than HDC (Figure 2) and similar to Big-foot.

In summary, the acceleration history of the fuel-ablator interface can be an important stabilizing lever, as it limits unbounded RM growth to an oscillatory behavior. This could have been responsible for the favorable performance of the Big-foot experiments compared to lower adiabat designs with conventional shock-timing. Since designs with conventional shock-timing continue to be used, delivering increased fusion output at larger scale, this work suggests further improvements are possible by reducing the growth during the Richtmyer-Meshkov period. Future designs can specifically seek to impose an acceleration, through an increasing ablation-pressure history or through shock mergers like seen in the Big-foot design.

This work was performed under the auspices of the U.S. Department of Energy by the Lawrence Livermore National Laboratory under Contract No. DE-AC52-07NA27344 and by General Atomics under Contract No. DE-NA0001808. This document was prepared as an account of work sponsored by an agency of the United States government. Neither the United States government nor Lawrence Livermore National Security, LLC, nor any of their employees makes any warranty, expressed or implied, or assumes any legal liability or responsibility for the accuracy, completeness, or usefulness of any information, apparatus, product, or process disclosed, or represents that its use would not infringe privately owned rights. Reference herein to any specific commercial product, process, or service by trade name, trademark, manufacturer, or otherwise does not necessarily constitute or imply its endorsement, recommendation, or favoring by the United States government or Lawrence Livermore National Security, LLC. The views and opinions of authors expressed herein do not necessarily state or reflect those of the United States government or Lawrence Livermore National Security, LLC, and shall not be used for

advertising or product endorsement purposes. LLNL-JRNL-835347

- [1] J. Lindl, “Development of the indirect-drive approach to inertial confinement fusion and the target physics basis for ignition and gain,” *Physics of Plasmas*, vol. 2, no. 11, p. 3933, 1995, doi: 10.1063/1.871025.
- [2] S. Atzeni and J. Meyer-ter-Vehn, *The Physics of Inertial Fusion: Beam-Plasma Interaction, Hydrodynamics, Hot Dense Matter*. in International Series of Monographs on Physics. Oxford: Oxford University Press, 2004. doi: 10.1093/acprof:oso/9780198562641.001.0001.
- [3] G. H. Miller, E. I. Moses, and C. R. Wuest, “The National Ignition Facility,” *Opt. Eng.*, vol. 43, no. 12, pp. 2841–2853, 2004, doi: 10.1117/1.1814767.
- [4] E. I. Moses, R. N. Boyd, B. A. Remington, C. J. Keane, and R. Al-Ayat, “The National Ignition Facility: Ushering in a new age for high energy density science,” *Physics of Plasmas*, vol. 16, p. 041006, 2009, doi: 10.1063/1.3116505.
- [5] M. L. Spaeth, K. R. Manes, D. H. Kalantar, and P. E. Miller, “Description of the NIF Laser,” *Fusion Science and Technology*, vol. 69, no. 1, pp. 25–145, Feb. 2016, doi: 10.13182/FST15-144.
- [6] J. Biener *et al.*, “Diamond spheres for inertial confinement fusion,” *Nuclear Fusion*, vol. 49, no. 11, p. 112001, 2009.
- [7] C. Dawedit *et al.*, “Grain size dependent physical and chemical properties of thick CVD diamond films for high energy density physics experiments,” *Diamond and Related Materials*, vol. 40, pp. 75–81, Nov. 2013, doi: 10.1016/j.diamond.2013.10.001.
- [8] O. L. Landen *et al.*, “Fuel convergence sensitivity in indirect drive implosions,” *Physics of Plasmas*, vol. 28, no. 4, p. 042705, Apr. 2021, doi: 10.1063/5.0033256.
- [9] B. A. Hammel *et al.*, “High-mode Rayleigh-Taylor growth in NIF ignition capsules,” *High Energy Density Physics*, vol. 6, no. 2, pp. 171–178, 2010.
- [10] C. R. Weber *et al.*, “First Measurements of Fuel-Ablator Interface Instability Growth in Inertial Confinement Fusion Implosions on the National Ignition Facility,” *Phys. Rev. Lett.*, vol. 117, no. 7, p. 075002, Aug. 2016, doi: 10.1103/PhysRevLett.117.075002.
- [11] L. Berzak Hopkins *et al.*, “Increasing stagnation pressure and thermonuclear performance of inertial confinement fusion capsules by the introduction of a high-Z dopant,” *Physics of Plasmas*, vol. 25, no. 8, p. 080706, Aug. 2018, doi: 10.1063/1.5033459.
- [12] D. H. Munro *et al.*, “Shock timing technique for the National Ignition Facility,” *Physics of Plasmas (1994-present)*, vol. 8, no. 5, pp. 2245–2250, May 2001, doi: 10.1063/1.1347037.
- [13] S. Le Pape *et al.*, “Fusion Energy Output Greater than the Kinetic Energy of an Imploding Shell at the National Ignition Facility,” *Phys. Rev. Lett.*, vol. 120,

- no. 24, p. 245003, Jun. 2018, doi: 10.1103/PhysRevLett.120.245003.
- [14] A. L. Kritcher *et al.*, “Achieving record hot spot energies with large HDC implosions on NIF in HYBRID-E,” *Physics of Plasmas*, vol. 28, no. 7, p. 072706, Jul. 2021, doi: 10.1063/5.0047841.
- [15] A. L. Kritcher *et al.*, “Design of inertial fusion implosions reaching the burning plasma regime,” *Nat. Phys.*, vol. 18, no. 3, Art. no. 3, Mar. 2022, doi: 10.1038/s41567-021-01485-9.
- [16] Indirect Drive ICF Collaboration *et al.*, “Lawson Criterion for Ignition Exceeded in an Inertial Fusion Experiment,” *Phys. Rev. Lett.*, vol. 129, no. 7, p. 075001, Aug. 2022, doi: 10.1103/PhysRevLett.129.075001.
- [17] A. L. Kritcher *et al.*, “Design of an inertial fusion experiment exceeding the Lawson criterion for ignition,” *Phys. Rev. E*, vol. 106, no. 2, p. 025201, Aug. 2022, doi: 10.1103/PhysRevE.106.025201.
- [18] A. B. Zylstra *et al.*, “Experimental achievement and signatures of ignition at the National Ignition Facility,” *Phys. Rev. E*, vol. 106, no. 2, p. 025202, Aug. 2022, doi: 10.1103/PhysRevE.106.025202.
- [19] Thomas, C. A., *Bulletin of the American Physical Society*, vol. 61, no. 18, 2016.
- [20] K. L. Baker *et al.*, “High-Performance Indirect-Drive Cryogenic Implosions at High Adiabatic on the National Ignition Facility,” *Phys. Rev. Lett.*, vol. 121, no. 13, p. 135001, Sep. 2018, doi: 10.1103/PhysRevLett.121.135001.
- [21] D. T. Casey *et al.*, “The high velocity, high adiabat, ‘Bigfoot’ campaign and tests of indirect-drive implosion scaling,” *Physics of Plasmas*, vol. 25, no. 5, p. 056308, Mar. 2018, doi: 10.1063/1.5019741.
- [22] S. W. Haan *et al.*, “Point design targets, specifications, and requirements for the 2010 ignition campaign on the National Ignition Facility,” *Physics of Plasmas*, vol. 18, no. 5, p. 051001, 2011, doi: 10.1063/1.3592169.
- [23] B. M. Haines *et al.*, “Robustness to hydrodynamic instabilities in indirectly driven layered capsule implosions,” *Physics of Plasmas*, vol. 26, no. 1, p. 012707, Jan. 2019, doi: 10.1063/1.5080262.
- [24] B. M. Haines *et al.*, “A mechanism for reduced compression in indirectly driven layered capsule implosions,” *Physics of Plasmas*, vol. 29, no. 4, p. 042704, Apr. 2022, doi: 10.1063/5.0083299.
- [25] M. M. Marinak *et al.*, “Three-dimensional HYDRA simulations of National Ignition Facility targets,” *Physics of Plasmas*, vol. 8, no. 5, p. 2275, 2001, doi: 10.1063/1.1356740.
- [26] S. J. Ali *et al.*, “Probing the seeding of hydrodynamic instabilities from nonuniformities in ablator materials using 2D velocimetry,” *Physics of Plasmas*, vol. 25, no. 9, p. 092708, Sep. 2018, doi: 10.1063/1.5047943.
- [27] V. A. Smalyuk *et al.*, “Review of hydrodynamic instability experiments in inertially confined fusion implosions on National Ignition Facility,” *Plasma Phys. Control. Fusion*, vol. 62, no. 1, p. 014007, Oct. 2019, doi: 10.1088/1361-6587/ab49f4.
- [28] C. Weber, “Understanding the impact of ablator microstructure and fuel-ablator mixing on ICF implosions,” *Bulletin of the American Physical Society*, vol. 2019, p. GI3.001, Jan. 2019.
- [29] S. Davidovits, C. R. Weber, and D. S. Clark, “Modeling and fuel-ablator mixing dynamics for perturbations driven by small-scale ablator inhomogeneity,” *Physics of Plasmas*, vol. in prep..
- [30] S. V. Weber *et al.*, “Simulations of indirectly driven gas-filled capsules at the National Ignition Facility,” *Physics of Plasmas (1994-present)*, vol. 21, no. 11, p. 112706, Nov. 2014, doi: 10.1063/1.4901598.
- [31] G. Dimonte and R. Tipton, “K-L turbulence model for the self-similar growth of the Rayleigh-Taylor and Richtmyer-Meshkov instabilities,” *Phys. Fluids*, vol. 18, no. 8, p. 085101, 2006, doi: 10.1063/1.2219768.
- [32] D. Besnard, F. H. Harlow, R. M. Rauenzahn, and C. Zemach, “Turbulent Transport Equations for Variable-Density Turbulence and Their Relationship to Two-Field Models,” Los Alamos National Laboratory, LA-12303-MA, 1992. [Online]. Available: <http://library.lanl.gov/cgi-bin/getfile?00193523.pdf>
- [33] B. E. Morgan, O. Schilling, and T. A. Hartland, “Two-length-scale turbulence model for self-similar buoyancy-, shock-, and shear-driven mixing,” *Phys. Rev. E*, vol. 97, no. 1, p. 013104, Jan. 2018, doi: 10.1103/PhysRevE.97.013104.
- [34] Y. Zhou, G. Zimmerman, and E. Burke, “Formulation of a two-scale transport scheme for the turbulent mix induced by Rayleigh-Taylor and Richtmyer-Meshkov instabilities,” *Phys. Rev. E*, vol. 65, no. 5, May 2002, doi: 10.1103/PhysRevE.65.056303.
- [35] G. Dimonte, “Spanwise homogeneous buoyancy-drag model for Rayleigh-Taylor mixing and experimental evaluation,” *Physics of Plasmas*, vol. 7, pp. 2255–2269, 2000.
- [36] B. Bachmann *et al.*, “Measurement of Dark Ice-Ablator Mix in Inertial Confinement Fusion,” *Phys. Rev. Lett.*, vol. 129, no. 27, p. 275001, Dec. 2022, doi: 10.1103/PhysRevLett.129.275001.
- [37] Lord Rayleigh, *Investigation of the Character of the Equilibrium of an Incompressible Heavy Fluid of Variable Density*, vol. s1-14. 1882. [Online]. Available: <http://plms.oxfordjournals.org>
- [38] G. Taylor, *The Instability of Liquid Surfaces when Accelerated in a Direction Perpendicular to their Planes. I*, vol. 201. The Royal Society, 1950. [Online]. Available: <http://www.jstor.org/stable/98398>
- [39] Y. Zhou, “Rayleigh-Taylor and Richtmyer-Meshkov instability induced flow, turbulence, and mixing. I,” *Physics Reports*, vol. 720–722, pp. 1–136, Dec. 2017, doi: 10.1016/j.physrep.2017.07.005.
- [40] Y. Zhou, “Rayleigh-Taylor and Richtmyer-Meshkov instability induced flow, turbulence, and mixing. II,” *Physics Reports*, Sep. 2017, doi: 10.1016/j.physrep.2017.07.008.

- [41] R. D. Richtmyer, “Taylor instability in shock acceleration of compressible fluids,” *Communications on Pure and Applied Mathematics*, vol. 13, no. 2, pp. 297–319, 1960, doi: 10.1002/cpa.3160130207.
- [42] E. E. Meshkov, “Instability of a shock wave accelerated interface between two gases,” *NASA Technical Translation*, vol. 13, pp. 1–14, 1970.
- [43] V. N. Goncharov, P. McKenty, S. Skupsky, R. Betti, R. L. McCrory, and C. Cherfils-Cl  rouin, “Modeling hydrodynamic instabilities in inertial confinement fusion targets,” *Phys. Plasmas*, vol. 7, no. 12, p. 5118, 2000, doi: 10.1063/1.1321016.
- [44] G. Dimonte, P. Ramaprabhu, and M. Andrews, “Rayleigh-Taylor instability with complex acceleration history,” *Physical Review E*, vol. 76, no. 4, p. 46313, 2007.
- [45] G. Dimonte and M. Schneider, “Density ratio dependence of Rayleigh–Taylor mixing for sustained and impulsive acceleration histories,” *Physics of Fluids*, vol. 12, p. 304, 2000.
- [46] J. Ding, T. Si, J. Yang, X. Lu, Z. Zhai, and X. Luo, “Measurement of a Richtmyer-Meshkov Instability at an Air- $\text{SF}_6$  Interface in a Semiannular Shock Tube,” *Phys. Rev. Lett.*, vol. 119, no. 1, p. 014501, Jul. 2017, doi: 10.1103/PhysRevLett.119.014501.
- [47] X. Luo *et al.*, “Long-term effect of Rayleigh–Taylor stabilization on converging Richtmyer–Meshkov instability,” *Journal of Fluid Mechanics*, vol. 849, pp. 231–244, Aug. 2018, doi: 10.1017/jfm.2018.424.
- [48] F. Chen, A. Xu, and G. Zhang, “Collaboration and competition between Richtmyer-Meshkov instability and Rayleigh-Taylor instability,” *Physics of Fluids*, vol. 30, no. 10, p. 102105, 2018.
- [49] M. Vandenboomgaerde, C. M  gler, and S. Gauthier, “Impulsive model for the Richtmyer-Meshkov instability,” *Physical Review E*, vol. 58, no. 2, pp. 1874–1882, Aug. 1998, doi: 10.1103/PhysRevE.58.1874.
- [50] M. Lombardini, D. I. Pullin, and D. I. Meiron, “Turbulent mixing driven by spherical implosions. Part 1. Flow description and mixing-layer growth,” *Journal of Fluid Mechanics*, vol. 748, pp. 85–112, 2014, doi: 10.1017/jfm.2014.161.
- [51] M. Flaig, D. Clark, C. Weber, D. L. Youngs, and B. Thornber, “Single-mode perturbation growth in an idealized spherical implosion,” *Journal of Computational Physics*, vol. 371, pp. 801–819, Oct. 2018, doi: 10.1016/j.jcp.2018.06.014.
- [52] N. J. Zabusky, J. Ray, and R. Samtaney, “Vortex Models for Richtmyer-Meshkov Fast/Slow Environments: Scaling Laws for Interface Growth Rates,” in *Proceedings of the Fifth International Workshop on Compressible Turbulent Mixing*, Stony Brook, 1996. [Online]. Available: [http://www.iwpctm.org/proceedings/IWPCTM5/papers/Zabusky\\_Ray\\_Samtaney.pdf](http://www.iwpctm.org/proceedings/IWPCTM5/papers/Zabusky_Ray_Samtaney.pdf)
- [53] L. A. Pickworth *et al.*, “Development of new platforms for hydrodynamic instability and asymmetry measurements in deceleration phase of indirectly driven implosions on NIF,” *Physics of Plasmas*, vol. 25, no. 8, p. 082705, Aug. 2018, doi: 10.1063/1.5039744.
- [54] A. L. Velikovich *et al.*, “Multi-mode hydrodynamic evolution of perturbations seeded by isolated surface defects,” *Physics of Plasmas*, vol. 27, no. 10, p. 102706, Oct. 2020, doi: 10.1063/5.0020367.
- [55] U. Alon, J. Hecht, D. Ofer, and D. Shvarts, “Power laws and similarity of Rayleigh–Taylor and Richtmyer-Meshkov mixing fronts at all density ratios,” *Physical review letters*, vol. 74, no. 4, pp. 534–537, 1995.
- [56] D. Ofer, U. Alon, D. Shvarts, R. L. McCrory, and C. P. Verdon, “Modal model for the nonlinear multimode Rayleigh–Taylor instability,” *Phys. Plasmas*, vol. 3, no. 8, p. 3073, 1996, doi: 10.1063/1.871655.
- [57] A. W. Cook and P. E. Dimotakis, “Transition stages of Rayleigh–Taylor instability between miscible fluids,” *Journal of Fluid Mechanics*, vol. 443, pp. 69–99, 2001.
- [58] J. R. Ristorcelli and T. T. Clark, “Rayleigh Taylor turbulence: self-similar analysis and direct numerical simulations,” *Journal of Fluid Mechanics*, vol. 507, pp. 213–253, May 2004, doi: 10.1017/S0022112004008286.
- [59] J. H. Eggert *et al.*, “Melting temperature of diamond at ultrahigh pressure,” *Nat Phys*, vol. 6, no. 1, pp. 40–43, Jan. 2010, doi: 10.1038/nphys1438.
- [60] D. S. Clark *et al.*, “Exploring implosion designs for increased compression on the National Ignition Facility using high density carbon ablators,” *Physics of Plasmas*, vol. 29, no. 5, p. 052710, May 2022, doi: 10.1063/5.0087052.
- [61] A. Do and others, “Direct measurement of ice-ablator interface motion for instability mitigation in indirect drive ICF implosions,” *Physical Review Letters*, in review.
- [62] R. Tommasini and et al, “Increased compression in HDC-based ablator implosions using modified dopant and drive profile,” *Physical Review Letters*, in preparation.